

## **Synthesis and characterization Al<sub>2</sub>O<sub>3</sub>-ZrO<sub>2</sub> bio-nanostructures with sintering effect, residual and thermally stable analysis**

M. F. Wasim<sup>a,b,\*</sup>, S. Ali<sup>a</sup>, M. W. Ashraf<sup>a,\*</sup>, A. Rafique<sup>c</sup>, J. Ahmad<sup>d</sup>, M. I. Akhter<sup>e</sup>,  
A. Qadeer<sup>a</sup>, S. Tayyaba<sup>f</sup>, Z. Ahmad<sup>g</sup>

<sup>a</sup>*Department of Physics, GC University, Lahore, Pakistan*

<sup>b</sup>*Department of Physics, Govt. Dyal Singh Graduate College, Lahore, Pakistan*

<sup>c</sup>*Department of Physics, Lahore Garrison University, Lahore, Pakistan*

<sup>d</sup>*Department of Mechanical Engineering, University of Engineering and Technology, Lahore-RCET Campus, Pakistan*

<sup>e</sup>*Department of Chemistry, GC University, Lahore, Pakistan*

<sup>f</sup>*Department of Computer Engineering, The University of Lahore, Pakistan*

<sup>g</sup>*Center for Advanced Materials (CAM), Qatar University, 2713, Doha, Qatar*

The thermal stability of nano composite materials is the important aspect of the modern era. In the advance modern devices, the nanostructures and nano composite material are used for the biological and other applications. The aluminum oxide is the most prominent oxides and composite at nano scale that show different structures, electrical and thermal properties which make it useful in different applications. Sol-Gel technique was used for synthesis to grow these nanostructures of Al<sub>2</sub>O<sub>3</sub>-ZrO<sub>2</sub>. Thermal stability was achieved and thermo-gravimetric (TGA) graphical analysis of synthesized material was performed. Size, phase and structure validation about the productive material was studied by X-Ray diffraction powder technique. Reaction completion and idea about annealing temperature of the synthesized material had pointed out by DSC-TGA (SDT) graphical peaks. Effect of the temperatures with equal variation from 500 °C, 700 °C, 900 °C and 1100 °C was performed to achieve the target thermal stability. Thermal analysis was also conducted in ANSYS workbench to visualize the thermal distributes like heat flux through the material. Optical properties such as band gap variation with temperature were studied by UV-vis analysis. Fourier transform infrared (FTIR) analysis was also performed. This work provides useful information related to nanostructures with sintering effect, residual and thermally stable analysis.

(Received May 10, 2021; Accepted September 4, 2021)

*Keywords: Al<sub>2</sub>O<sub>3</sub>-ZrO<sub>2</sub>, Bio-nanostructures, TGA-Residual, Wet-chemical, Ansys simulation*

### **1. Introduction**

Nanoparticles of the metal oxide have attracted for advanced technological device and industrial applications due to the interesting properties. Due to its lots of application of the nano composite now a days in the ceramic and crucible material industry have got a great importance. It is used for the surface coating, thermal interfacing and surface insulating. The Zirconia-toughened alumina (ZTA) has great ceramic behavior and the thermal stable properties. On the base of its some physical properties such as the toughness related the strength, the resistive ability related to wear and tear, softness related to malleable application in the engineering industries [1]. In this paper we study the thermal properties of the ZTA experimentally and theoretically by fuzzy logics techniques, ceramic are compounds that may be classified into metallic and nonmetallic elements. They are resistance to the high temperature and the corrosion environment that most metals have. These are used to create the bones and tooth replacements, super strong cutting tools. Or to conduct the heat and electricity [2]. It is notable that both the crack durability and the strength of

---

\* Corresponding author: rfwasim@yahoo.com

alumina pottery. These properties are improved altogether by the scattering of 10–20 vol. % of meta-stable tetragonal (t) zirconia particles. To this reason, the content of the zirconium oxide into final product respectively changes as the regular behavior to check and controlled the variation on the other components such as a rule utilizing 2 mol% yttrium chloride to some extent balance out the tetragonal stage [3, 4]. The degree of hardening these composites are under system studies. Such synthesized accomplished material and these composites rely upon the molecule size. This revealed that the variation in the weight ratio of the  $\text{Al}_2\text{O}_3$  other constituent Zirconium chloride salt to achieve the content of the  $\text{ZrO}_2$ . The structures of the synthesized material has phase of the tetragonal with meta-stable behavior. Both constituents groups such as  $\text{Al}_2\text{O}_3$  and  $\text{ZrO}_2$  would not just upgrade the odds of a uniform  $\text{Al}_2\text{O}_3$  and  $\text{ZrO}_2$  circulation, yet it like wise expands the chance of  $\text{ZrO}_2$  being held as meta-stable tetragonal stage. A significant issue had accomplished a reaction about the synthesis of  $\text{Al}_2\text{O}_3$ – $\text{ZrO}_2$  bio-nanostructures. The annealing effect on the composite nano-synthesized material has studied in detail on the base of the mention characteristics. Unfavorably influence has the densification conduct, yet additionally will diminish the held tetragonal  $\text{ZrO}_2$  [5].

In the present study the annealing effect on the morphology, phase, size and band gap on the synthesized bio-nano structures of the uniformly textures  $\text{Al}_2\text{O}_3$ – $\text{ZrO}_2$  composite. The wet-chemical technique sol-gel had used to achieve the required productive synthesized material. Stability of the reaction has achieved by the addition of the Yttrium chloride. A homogenous blend with nano-sized powder has achieved, annealed and put for the characterization. The novelty of the work achieves the nanostructures with yttrium stabilizing and annealing effect details study with its thermal stability parameters. All the data and the analysis have interrelated graphically and statistically in details. The temperature selection about start and end treatment has decided on the base of the TGA-DSC analysis [5, 6].

## 2. Thermal Analysis using ANSYS

Thermal analysis of  $\text{Al}_2\text{O}_3$ – $\text{ZrO}_2$  was performed by making 3D sheet. The analysis was performed using ANSYS workbench. After creating sheet the material properties and element were define to total heat flux and directional heat flux through the 3D geometry. The solution was obtained by changing the condition 500 °C, 700 °C, 900 °C and 1100 °C. The total heat flux is shown in Fig. 1.

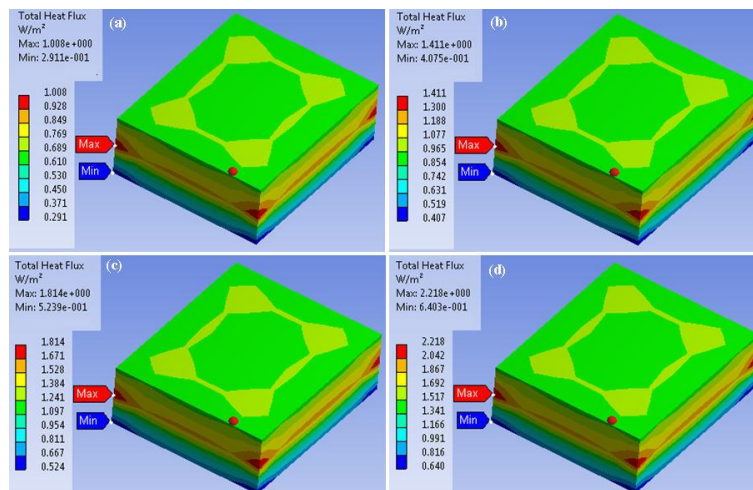


Fig. 1. Total Heat Flux (a) at 500 °C (b) at 700 °C (c) at 900 °C (d) at 1100 °C.

The directional heat flux through the 3D sheet is shown in Fig. 2. Red color shows maximum values at certain point and blue color shows minimum values at corresponding point. When load is applied the structure bends to opposite.

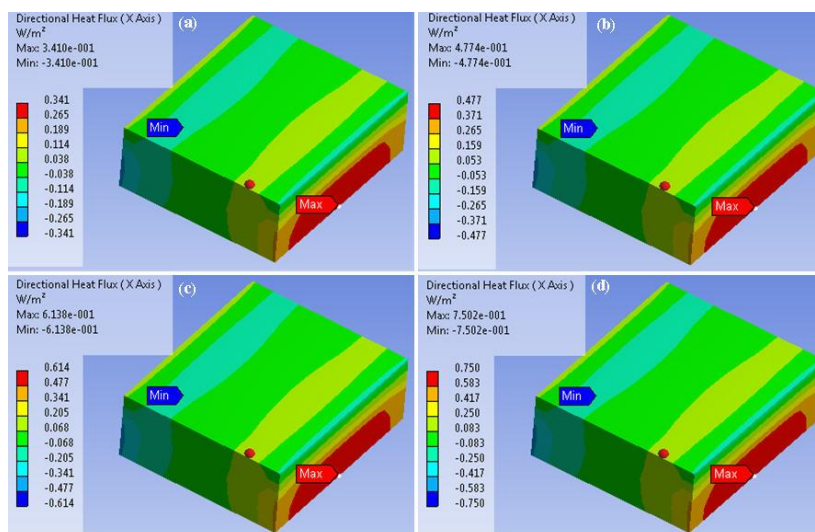


Fig. 2. Directional Heat Flux (a) at 500 °C (b) at 700 °C (c) at 900 °C (d) at 1100 °C.

### 3. Experimental procedure

As a matter of first step, we set up the 0.5 molar arrangement of solution for Zirconium Chloride Dihydrate ( $ZrOCl_2 \cdot 8H_2O$ ) in a cone shaped cup which is put on the hot plate attractive stirrer string vivacious with speed 1500 fire up/min. In second arrangement of the solution for 0.5 M of Zirconium Chloride Dehydrate ( $ZrOCl_2 \cdot 8H_2O$ ) was ready. Both arrangement blended in an amount of 50 ml of this arrangement add in 50 ml of the Aluminum Nitrite arrangement solution, then, at that point add the 50 ml glycolic corrosive 0.5 M arrangement solution into these to two solution which is in the constant state attractive mixing by 4% load of yttrium chloride. The blended hydro gel was acquired get-togethers mixing for the 6nhours at 700 °C. We perform mixing magnetic stirring method for six hours, with constant alluring mixing round per minutes. Aluminum foil is used for covering the beakers, the reaction blend becomes obscure and a while later shows yellowish expression, which was dull first and foremost underneath offering a hint of nano silica creating. Blend was kept on blending for required time. The consistency of the pack bit by bit extended in conclusion set to a gel which was kept two days in drying process. The gel was centrifuged again and again. Than washed with foamed refined water to wipe out corruptions and filtered. The dried gel was done in the extent of 450–1200 °C with a warming speed of 10 °C/min. The Schematic diagram of synthesis setup is shown in Fig. 3.

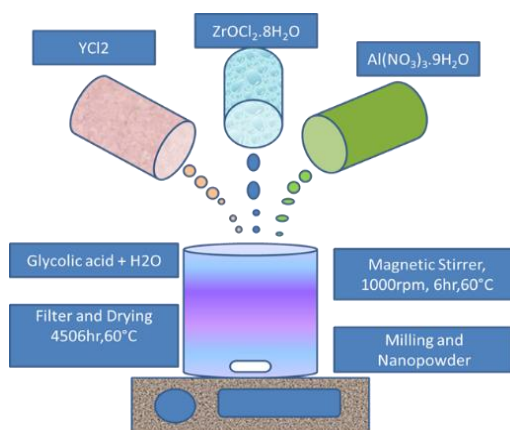


Fig. 3. Schematic diagram of the chemical reaction.

## 4. Result and discussion

### 4.1 XRD analysis

The Fig. 4 shows the graphical information about XRD analysis combined entire samples. All the samples coded properly with indication of the temperature on the figures. Tetragonal phase of the synthesized material has confirmed by the XRD analysis. X, pert High score had developed a close agreement with, “Aluminum Zirconium oxide-00-054-00294” reference model. The Broadening of the peaks and sharpness behavior about the xrd analysis has increasing effect. This indication was about the positive change in its size [2, 7]. All the samples have the homogeneous and uniform, up and down peaks expression with basic peak indication at 3000 °C. Miller indices plans representation (110) has notice in calculation for the calculation of the average particle size of the synthesized bio-nanostructures which shows the close association with SEM analysis. The All the samples common behavior peaks was observed at the (11 0), its broadening calculation, intensity observation implemented by the Scherer’s equation to find average size that is found to be 10-15nm. Homogeneity and uniformity shows the perfection and controlled parameters in all the methodology [8]. This marvel is because of higher explicit surface space of nano-powder delivered from AZ-F forerunners contrasted with one created from AZ-F. The power of these stages increments up to 1100 °C. The development of  $\alpha$ -Al<sub>2</sub>O<sub>3</sub> stage is finished at 1100 °C in the two examples. The change of momentary alumina to  $\alpha$ -alumina happens at higher temperatures within the sight of zirconium [9].Phase  $\alpha$ -Al<sub>2</sub>O<sub>3</sub> uniform formation was also a indication of the XRD uniform textures behavior that remains constant about all temperature from 500 °C to 1100 °C. The conversion of midway ceramic alumina to  $\alpha$ -alumina happen at higher temperature up to turns in the presence of zirconium[5, 10].

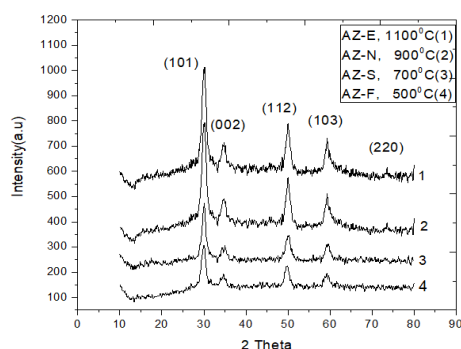


Fig. 4. XRD analysis pattern of all the samples.

### 4.2. Thermal behavior

The thermal stability and the annealing temperature assessment was carried with the SDT Q600 instrument which have proficiency in its simultaneously analysis ability regarding the TGA and DSC with a powdery form. Phase’s changes alterations have observed during this analysis and data interpretation. This analysis was performed to study the phase changes that occurred during the heat treatment of composite materials. From the start of heating, the weight loss carried out upto  $\Delta m = 19.04\%$  of initial amounts on reaching to 350 °C. This reduction is the effect of evaporation of water and moisture from the synthesized material (at 1000 °C). After evaporation of water , the decomposition of the absorbed or developed CO<sub>2</sub> and CO because its melting temperature stand within 175 °C to 200 °C [11]. In the second, from the surface organic substance polyvinyl pyrrolidone (pvp) was desorption and decomposition which cause a mass loss  $\Delta m = 33.14\%$  from the sampled material. The next one step gives a positive variation and increase mass. The essential drive in the wake of it mass increase was oxidation of the material from 650-1000 °C. The residual effect and the thermal stability of bio-nanostructure had achieved. The residue product synthesized material was of 48% on heating up to 1000 °C which shows that at the temperature more than of this no phase change variation happen that’s shows its stability [12]. Weight loss indication also done due to the process of the sublimation in nano-synthesized

material. A smooth behavior in the curves both for the TGA and DSC was an assessment about end of further phase changes of decomposition which also shows the end of reaction. Due to high melting and boiling point of reactants was the starting material upto 1800 °C. So the analysis contains the peaks of the dehydrated salt and alkoxide gels in Fig. 5 and Fig. 6 corresponding.

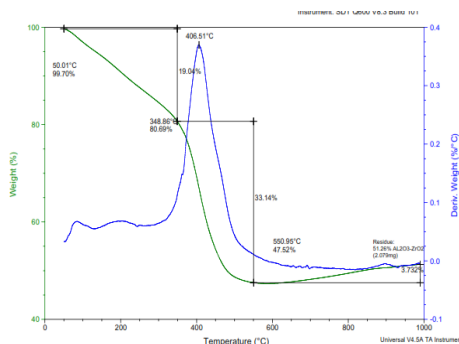


Fig. 5. DSC/TGA analysis of the sample for the sintering temperature analysis.

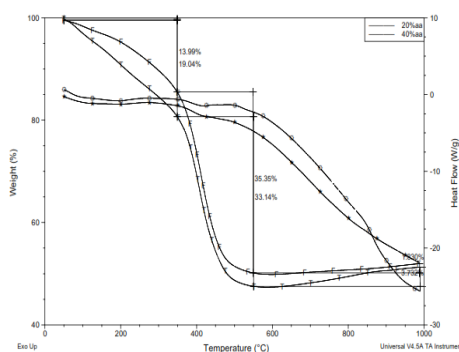


Fig. 6. Comparison DSC/TGA of the both the samples.

Above figures showed the graph between weight losses, heat flow with common variation of temperature from 0-100 °C. The derivative over the plot shows the maximum decomposition point which was found to be at 45 °C. The figures 5 show that the changes behavior of the synthesized material and the variation loop area and the other decomposition as marked over the graph. Small phase changes occur due to the low content, the XRD innovation could not show by the curves. The big reduction of 46% in weight was observed in the TG curve. Figs. 6 describes the detailed correlation of TG curves and DTA curves of all examples [13]. For thermogravimetric characteristics deliberate reduction of about 34% weight over the temperature of 970 °C. Residual amount at the end of the analysis is the indication of the following, for example, the glycol component, after polymerization and expulsion of side effects from the metal oxide order measurement. The DTA curve shows peaks related to the endothermic reaction at the 80C. It's also a justification about the polymerization and residual amount of the synthesized material. Exothermic hump has observed at 276 °C that was indication about the metallic oxides evolution of the starting reacting substance [12, 13]. The evaluation effects and the correlation between TG curves and DTA curves for the corresponding samples briefed as follows: Crystallization were independent all endothermic observed in both samples at 300-1000 °C, which can be observed in above figures. The maximum change occurs at maximum temperature about 450 °C. Comparison of the DTA curves for all analysis, the onset of metal oxide formation in two samples which shows close correlation with the XRD analyzes of the samples [14].

### 4.3. FTIR analysis

The significant pinnacles showing up in the FTIR spectra of synthesized product framework which could be identified with the accompanying:

- (1) Surface adsorbed water function group indicated as –OH extending vibration
- (2) Surface reinforced water function group indicated as –OH twisting vibration
- (3) Primary water related, M-OH bonding, shown by –OH extending vibration
- (4) Underlying water related, M-OH bonding, shown by –OH twisting vibration
- (5) Vibration of extending mode related to I–O
- (6) Vibration of extending mode related to Zr–O

The Fig. 7 shows the functional groups related modes of vibration of all functional group present in the synthesized materials. From the wavenumber range 3136–3857  $\text{cm}^{-1}$  that's related to the vibration mode of extending behaviors of the atomic vibrations of the water molecules adsorbed in the surface [15]. Other peaks related to the functional groups are mentioned in the above six points. The downward hump and valley has observed which indicated the –OH bonding levels. The hump of the vella and the depth has decreases with increases of the samples [16].

The finger prints related to the Al-OH functional groups also have its bending occurrence from the region of the straight behavior with many others bending modes. Similarly the Zr-OH with its twisting and extending behaviors shows its presence from the straight curves of the range 3000-1700  $\text{cm}^{-1}$ . Because the above functional groups are the constituents of the reactants and annealed, so these attains its reduction to a minimum level [17].

The water molecules attachment of the functional groups also correlated its physical attachments such a surface water molecules mode of vibration. Secondly the underlying mode of the vibration with both extending and twisting behaviors. Third one is the adsorbed based attachments of the modes of vibration that's physically attachment with M link radicals such as Zr and Al. The dipole movement fixation with lattice vibration shows its continuous that the basic parameter of the composite materials synthesis [18]. This communication most likely outcomes in the decrease of vibrational dipole second in twisting consequently making a more noteworthy power of fascination on the extending vibration. The extending vibration for underlying –OH and adsorbed water shows up at wave number more prominent than 3000  $\text{cm}^{-1}$ . A cautious examination of extending frequencies uncover that an increment in ZrO<sub>2</sub> content in the cluster causes a critical change in the –OH extending design upto 10% ZrO<sub>2</sub> expansion for A5Z to A10Z tests. Four pinnacles are noticed in the wave number reach 3656, 3553, 3471 and 3146  $\text{cm}^{-1}$  which represent –OH extending. In the A15Z tests two additional extra pinnacles show up at 3857 and 3425  $\text{cm}^{-1}$ , which demonstrate the presence of more –OH in this group [19].

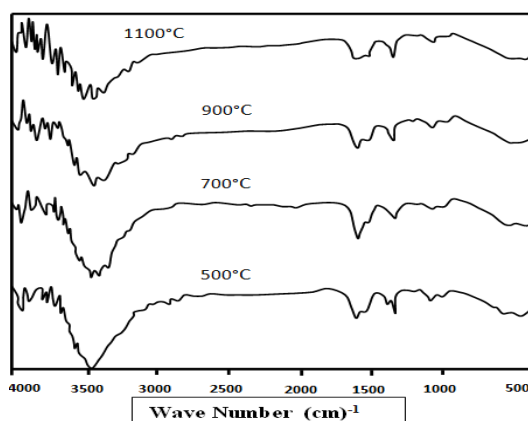


Fig. 7. FTIR of samples sintered at different temperatures.

The three deep peaks have observed in the range of 1700-900  $\text{cm}^{-1}$ . The peaks continuously show its decreasing downwards peaks respectively. This behavior has found

throughout in all the samples. The group  $-OH$  has its contribution about is controlling and broadening oscillating modes of the vibration also involve the coupling effect of these attached radicals of the synthesized material. Indications of the graphical appearance at points 1764, 1634 and  $1385\text{ cm}^{-1}$  correlated to the rotary vibration of  $Zr-OH$  get-togethers. The climax location of the curves is fundamentally impressive just about the common for all the models.  $Al-O$  vibration correlated finger print is found at the  $1070\text{ cm}^{-1}$  [18]. The strong digestion band of the last one may be credited to six-worked with  $Al_3+$  particles. The maintenance is band at  $1070\text{ cm}^{-1}$  is due to the presence of alumina-gel. The above results deduce that alumina in this particular alumina-zirconia system is accessible as a moderate bayerite. The  $-OH$  broadening and bowing vibrations is displayed by both the constituents of the hydro gels [20].

#### 4.4. UV-vis Spectroscopy analysis

The optical properties have its correlation about the electronics transition behavior. The Tauc relation has used for the calculation of the optical band gap Tauc relation which is given as

$$(\alpha h\nu)^{1/n} = A(h\nu - E_g)$$

where

$E_g$  = the band gap energy

$A$  = A constant of the materials

$n$  = exponent depends on the type of transition.

The model of spectrophotometer that utilized in the UVvis estimation has number CECIL2700. To accomplish the degree of assimilation in the splendid noticeable area [21]. The curves between frequencies versus optical thickness were recorded for every one of the eight models in the 280-650 nm range, as displayed in Fig. 8. Clearly, the ingestion diminishes with expanding recurrence for a given shape [22-25].

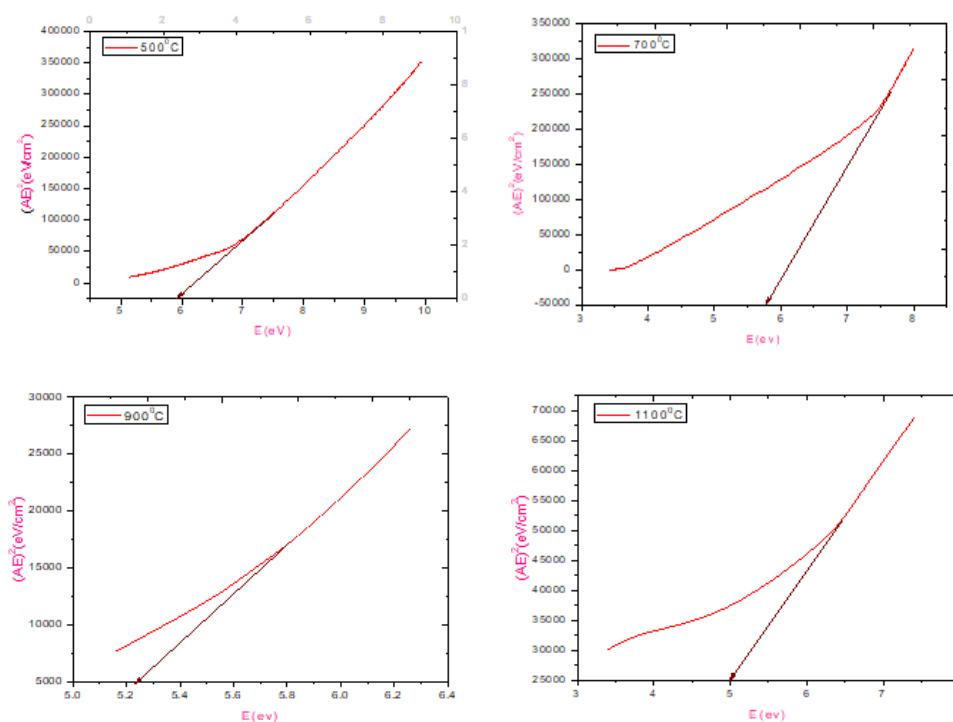


Fig. 8. Band gap determination of sample at different sintered temperature.

#### 4. Conclusion

In This work  $\text{Al}_2\text{O}_3\text{-ZrO}_2$  was synthesized using a simple Sol-Gel technique in presence of the constant Yttrium chloride stabilizer and Glycolic solution which confirms by X-Ray diffraction analysis. Size of particle also confirmed in the nano range and structure of the phase. XRD and Sherr,s formula techniques were used to inspect synthesis bio-nanostructure in range of 15-25 nm . Synthesized material has sintered at different temperatures  $500\text{ }^\circ\text{C}$ ,  $700\text{ }^\circ\text{C}$ ,  $900\text{ }^\circ\text{C}$  ,  $1100\text{ }^\circ\text{C}$  to study the structural, optical band gape behavior and thermal stability. ANSYS workbench was also used to study the heat flux through the material. The crystallinity has increase with increase of the temperatures. The thermal stability of the Synthesized  $\text{Al}_2\text{O}_3\text{-ZrO}_2$  nano composite materials has achieved  $1000\text{ }^\circ\text{C}$  with the help of the TGA. Synthesis of  $\text{Al}_2\text{O}_3\text{-ZrO}_2$  Bio-nanostructures has achieves indication based on DSC-TGA (SDT) analysis because its show its phase change peak at temperature ( $450\text{ }^\circ\text{C}$ ). The bandage was tuned in increasing aspect of the bandage which justify by UV-vis analysis FTIR analysis was used to check the possible functional group at different temperatures and their composition effects which has found at  $451\text{cm}^{-1}$ .

#### References

- [1] Bartolomé, J.F., et al., New  $\text{ZrO}_2/\text{Al}_2\text{O}_3$  Nanocomposite Fabricated from Hybrid Nanoparticles Prepared by  $\text{CO}_2$  Laser Co-Vaporization. *Scientific Reports*, 2016. 6(1): p. 20589.
- [2] Koltsov, I., et al., The new nano-enabled phase map of  $\text{ZrO}_2\text{-Al}_2\text{O}_3$ . *Scientific Reports*, 2019. 9(1): p. 5540.
- [3] Sarkar, D., S. Adak, and N.K. Mitra, Preparation and characterization of an  $\text{Al}_2\text{O}_3\text{-ZrO}_2$  nanocomposite, Part I: Powder synthesis and transformation behavior during fracture. *Composites Part A: Applied Science and Manufacturing*, 2007. 38(1): p. 124-131.
- [4] Ponkumar, S., et al.,  $\text{ZrO}_2\text{-Al}_2\text{O}_3$  nanocomposite: Synthesis, characterization and influence of electron beam irradiation on the structural and PL properties. *AIP Conference Proceedings*, 2018. 1966(1): p. 020009.
- [5] Yaghoubi, A., A. Ramazani, and S. Taghavi Fardood, Synthesis of  $\text{Al}_2\text{O}_3/\text{ZrO}_2$  Nanocomposite and the Study of Its effects on Photocatalytic Degradation of Reactive Blue 222 and Reactive Yellow 145 Dyes. *ChemistrySelect*, 2020. 5(32): p. 9966-9973.
- [6] Danilenko, I., et al., The Peculiarities of Structure Formation and Properties of Zirconia-Based Nanocomposites with Addition of  $\text{Al}_2\text{O}_3$  and NiO. *Nanoscale research letters*, 2017. 12(1): p. 125.
- [7] Fathy, A., O. Elkady, and A. Abu-Oqail, Production and properties of  $\text{Cu-ZrO}_2$  nanocomposites. *Journal of Composite Materials*, 2017. 52(11): p. 1519-1529.
- [8] Palmero, P., Structural Ceramic Nanocomposites: A Review of Properties and Powders' Synthesis Methods. *Nanomaterials*, 2015. 5(2): p. 656-696.
- [9] Niihara, K., New Design Concept of Structural Ceramics Nanocomposites. *Journal of the Ceramic Society of Japan*, 1991. 99(1154): p. 974-982.
- [10] Chebil, W., et al., Study of the growth time effect on the structural, morphological and electrical characteristics of  $\text{ZnO/p-Si}$  heterojunction diodes grown by solbath deposition method. *Journal of Alloys and Compounds*, 2019. 771: p. 448-455.[11] Mallakpour, S. and M. Dinari, Enhancement in thermal properties of poly(vinyl alcohol) nanocomposites reinforced with  $\text{Al}_2\text{O}_3$  nanoparticles. *Journal of Reinforced Plastics and Composites*, 2013. 32(4): p. 217-224.
- [12] Pashaei, S., S. Hosseinzadeh, and H. Hosseinzadeh, TGA investigation and morphological properties study of nanocrystalline cellulose/ag-nanoparticles nanocomposites for catalytic control of oxidative polymerization of aniline. *Polymer Composites*, 2019. 40(S1): p. E753-E764.
- [13] El Sayed, A.M., Synthesis, optical, thermal, electric properties and impedance spectroscopy studies on  $\text{P(VC-MMA)}$  of optimized thickness and reinforced with MWCNTs. *Results in Physics*, 2020. 17: p. 103025.

- [14] Thermal Properties of Polymer Nanocomposites, in Fundamentals, Properties, and Applications of Polymer Nanocomposites, J.H. Koo, Editor 2016, Cambridge University Press: Cambridge. p. 332-388.
- [15] Iaiche, S. and A. Djelloul, ZnO/ZnAl<sub>2</sub>O<sub>4</sub> Nanocomposite Films Studied by X-Ray Diffraction, FTIR, and X-Ray Photoelectron Spectroscopy. *Journal of Spectroscopy*, 2015. 2015: p. 836859.
- [16] Alharthi, F.A., et al., Facile one-pot green synthesis of Ag–ZnO Nanocomposites using potato peel and their Ag concentration dependent photocatalytic properties. *Scientific Reports*, 2020. 10(1): p. 20229.
- [17] Karami, H., M.A. Karimi, and R. Jokar, Application of ZnO-Al<sub>2</sub>O<sub>3</sub> Nanocomposite as Nanocatalyst for Photodegradation of Acid Violet 5B. *Journal of the Chinese Chemical Society*, 2015. 62(5): p. 449-455.
- [18] Aghaei, M., S. Sajjadi, and A.H. Keihan, Sono-coprecipitation synthesis of ZnO/CuO nanophotocatalyst for removal of parathion from wastewater. *Environmental Science and Pollution Research*, 2020. 27(11): p. 11541-11553.
- [19] Hosseini Largani, S. and M. Akbarzadeh Pasha, The effect of concentration ratio and type of functional group on synthesis of CNT–ZnO hybrid nanomaterial by an in situ sol–gel process. *International Nano Letters*, 2017. 7(1): p. 25-33.
- [20] Sheikh, M., M. Asghari, and M. Afsari, Effect of tiny amount of zinc oxide on morphological and thermal properties of nanocomposite PEBA thin films. *Alexandria Engineering Journal*, 2018. 57(4): p. 3661-3669.
- [21] Lin, T.-H., et al., Selectively enhanced band gap emission in ZnO/Ag<sub>2</sub>O nanocomposites. *Optics Express*, 2009. 17(6): p. 4342-4347.
- [22] Zhang, L., et al., ZIF-8 derived ZnO/Zn<sub>6</sub>Al<sub>2</sub>O<sub>9</sub>/Al<sub>2</sub>O<sub>3</sub> nanocomposite with excellent photocatalytic performance under simulated sunlight irradiation. *New Journal of Chemistry*, 2019. 43(7): p. 2990-2999.
- [23] Somraksa, W., et al., Physical and Photocatalytic Properties of CeO<sub>2</sub>/ZnO/ZnAl<sub>2</sub>O<sub>4</sub> Ternary Nanocomposite Prepared by Co-precipitation Method. *Materials Research*, 2020. 23.
- [24] Khalili, E. and S.A. Hassanzadeh-Tabrizi, ZnO–CdO nanocomposite: microemulsion synthesis and dye removal ability. *Journal of Sol-Gel Science and Technology*, 2017. 81(2): p. 475-482.
- [25] Yadav, S., et al., Low temperature synthesized ZnO/Al<sub>2</sub>O<sub>3</sub> nano-composites for photocatalytic and antibacterial applications. *Semiconductor Science and Technology*, 2020. 35(5): p. 055008.